

Numerical Simulations of a Spin Dynamics Model Based on a Path Integral Approach

Thomas Nussle,^{1,*} Stam Nocolis,^{2,†} and Joseph Barker^{1,‡}

¹*School of Physics and Astronomy, University of Leeds, Leeds, LS2 9JT, United Kingdom*

²*Institut Denis Poisson, Université de Tours, Université d'Orléans, CNRS (UMR7013), Parc de Grandmont, F-37200, Tours, France*

Inspired by path integral molecular dynamics, we build a spin model, in terms of spin coherent states, from which we can compute the quantum expectation values of a spin in a constant magnetic field. This formulation facilitates the description of a discrete quantum spin system in terms of a continuous classical model and recasts the quantum spin effects within the framework of path integrals. In particular, it allows for a much more direct path to the low- and high-temperature limits and to the definition of effective classical Hamiltonians. In this formalism, the quantum properties of the spins are described through an effective anisotropy. To check this, we solve the effective classical model using atomistic spin dynamics, we calculate thermodynamic observables and show that our effective classical models can reproduce accurate quantum expectation values within the relevant temperature ranges.

INTRODUCTION

Spin models of magnetic materials are usually either quantum or classical in terms of the elementary building blocks on which they are based. In quantum spin models, the spin states belong to the quantum space of states that includes all linear superpositions of the eigenstates of \hat{S}_z and the spin variables are quantum operators, whereas in classical spin models, the ‘spins’ are actually magnetic moments of fixed length. Even though there are semi-classical models which describe quantum models in terms of at least “partially classical” systems, the computed quantities are, in the end, classical objects.

Quantum models allow accurate calculation of both thermodynamics and dynamics, which intrinsically include purely quantum effects such as entanglement and quantum fluctuations. However, the size of systems that can be studied is often limited to tens or hundreds of spins due to the large computational cost, as solving quantum problems exactly amounts to diagonalization of larger and larger matrices, and even approximation schemes thereof suffer from scaling issues. Numerical methods, such as quantum Monte Carlo (QMC), allow calculations of very large quantum spin systems (hundreds of thousands of spins) with very high accuracy. However, there is no access to dynamical quantities, as QMC is intrinsically a description of thermodynamics, where time is absent. Other quantum methods which do provide access to real-time dynamics cannot provide results for such large systems. Additionally, fundamental issues also arise, such as the ‘sign problem’ in the case of antiferromagnets, since the Hubbard-Stratonovich transformation leads to an effective Hamiltonian that is not hermitian although the evolution operator is unitary¹.

Classical spin models are frequently used to study the dynamics and thermodynamics of magnetic materials, helping to interpret experiments at “high” temperatures, where quantum effects—such as entanglement—can be neglected. The computational cost is relatively low, and the formalism is easy to parallelize, leading to routine simulations of the dynamics of hundreds of thousands or even millions of spins. While these classical models give a good qualitative description of the magnetic dynamics, issues arise at lower temperatures,

where the assumption of classical Boltzmann statistics is no longer appropriate. The magnon Debye temperature tends to be very high and of the same size as the magnetic ordering temperature, so the ‘low-temperature’ regime may cover most of the temperature range of magnetic ordering^{2,3}. Recent efforts have been made to introduce ad hoc corrections to classical spin models to produce results that more closely resemble quantum models and to better agree with experimental measurements^{2,4-8}. However, these approaches are incapable of including quantum effects, such as tunneling between macroscopic states or zero-point fluctuations. These quantum effects are becoming relevant on larger length scales and higher temperatures, for example, with the measurement of the motion of domain walls induced by quantum domain fluctuations in Cr up to 40K⁹. Thus, what is still lacking is a dynamical quantum model whose accuracy can bridge the gap between a fully quantum simulation of a few atoms and an effective classical model and that enables simulations scalable to the size of spintronic device components of millions of spins.

Here, we describe a bridge between quantum and classical spin models by employing a path integral formalism for spin dynamics. This is inspired by path integral molecular dynamics¹⁰ where the efficiency of classical molecular dynamics is used to calculate quantum properties, by establishing the appropriate evolution equations to move in the phase space of the quantum system and thus sample configurations therein¹¹. However, how to take into account spin degrees of freedom and sample the corresponding phase space is by no means obvious.

First attempts to do so¹², in particular for molecular magnets¹³ express the spin degrees of freedom in terms of equivalent, though fictitious, position and momentum variables and using the known molecular dynamics formalism in this guise. Hence, these involve mapping the spin Hamiltonian to a particle Hamiltonian. This makes the interpretation of the results in terms of classical magnetic moments, the actual experimental observable, much less straightforward, and this mapping is difficult to build for more complex spin interactions. However, the real problem which we must overcome is that the space of positions and momenta is flat; while the space spanned by the spin degrees of freedom is curved.

It is this problem that is solved by using the basis of spin coherent states¹². While spin coherent states have been used in some quantum methods¹⁴, these methods incur a non-trivial cost, for large systems, as well as not being well-suited for extracting the information on the individual (classical) spin components.

We note that spin coherent states have also recently been used in methods to derive/rederive equations of motion for magnetization dynamics¹⁵.

In this Article we consider the simplest nontrivial spin system: a single spin in an external magnetic field, described by the Zeeman Hamiltonian. We develop a formalism which uses the spin coherent states and the operators that act on them to solve for some exact cases, and compare the results obtained to numerical calculations performed with classical atomistic spin dynamics methods, augmented with a field, which represents the quantized nature of the spins. We demonstrate that this formalism can take into account the quantum effects of the spin, across a broad range of temperatures, with deviations appearing only at “very low” temperatures, as expected by intuition.

I. FROM THE CLASSICAL SPIN STATES TO THE SPIN COHERENT STATES

In molecular dynamics, the dynamical variables of the quantum system take values in a flat space. This makes the application of path integrals using classical positions and momenta relatively straightforward. For spin systems, the dynamical variables, the components of spin, take values in a curved space and can only take discrete values due to the discrete spectrum of the spin Hamiltonian

$$\{|s, m\rangle\}, \quad m \in \llbracket -s, s \rrbracket, \quad (1)$$

where s is the principal quantum number and m labels all different possible states with this given spin s . For example, with $s = 2$ there are $2s + 1 = 5$ eigenstates:

$$\{|2, -2\rangle, |2, -1\rangle, |2, 0\rangle, |2, 1\rangle, |2, 2\rangle\}. \quad (2)$$

However, all possible states of a quantum system of spin $s = 2$ are linear combinations of these five states, i.e. they are described as

$$|\psi\rangle = c_{-2}|2, -2\rangle + c_{-1}|2, -1\rangle + c_0|2, 0\rangle + c_1|2, 1\rangle + c_2|2, 2\rangle \quad (3)$$

The normalization of these states implies that the coefficients satisfy the constraint

$$|c_{-2}|^2 + |c_{-1}|^2 + |c_0|^2 + |c_1|^2 + |c_2|^2 = 1, \quad (4)$$

which defines a point on the unit sphere in ten dimensions, but the property that five phases can be modded out reduces this to a five-dimensional manifold. The real challenge is to sample this space efficiently.

The partition function of this quantum spin system is the volume of this five-dimensional manifold, which is finite:

$$\mathcal{Z} = \int d^2c_{-2}d^2c_{-1}d^2c_0d^2c_1d^2c_2 \delta(|c_{-2}|^2 + |c_{-1}|^2 + |c_0|^2 + |c_1|^2 + |c_2|^2 - 1). \quad (5)$$

Upon coupling the magnetic moment to a thermal bath, the partition function takes the form

$$\mathcal{Z} = \int d\psi \langle \psi | e^{-\beta H} | \psi \rangle = \int d^2c_{-2}d^2c_{-1}d^2c_0d^2c_1d^2c_2 \delta(|c_{-2}|^2 + |c_{-1}|^2 + |c_0|^2 + |c_1|^2 + |c_2|^2 - 1) e^{-\beta H(c)}, \quad (6)$$

with $\beta = 1/(k_B T)$, where $k_B = 1.381 \times 10^{-23}$ J/K is the Boltzmann constant and T is the temperature in Kelvin. From Eq. (6) it is not obvious how the dynamical behavior of the quantum system, defined over the full manifold, goes over to that of a classical system, localized on the five states $\{|2, -2\rangle, |2, -1\rangle, |2, 0\rangle, |2, 1\rangle, |2, 2\rangle\}$, in the “classical limit” and how this can be defined.

This requires a careful discussion of what we mean by a ‘quantum’ system. On the one hand, we have the discrete basis of the eigenstates of the Hamiltonian, but on the other hand, we have the quantum superposition of states which leads to a continuous manifold of possible quantum states. Here, we emphasize that we are dealing with classical measurements of quantum systems, which means that the outcome of any single measurement can only be an eigenstate of our Hamiltonian—which is labeled by an integer for spin systems. The prototype of this situation is the experiment by Stern and Gerlach¹⁶, where, even though the possible quantum states of the electron can belong to a superposition,

$$|\psi\rangle = a|\uparrow\rangle + b|\downarrow\rangle, \quad (7)$$

such that $a^2 + b^2 = 1$, the outcome of the measurement of the experiment is either $|\uparrow\rangle$ or $|\downarrow\rangle$. This is in contrast to a classical measurement of the projection along the z -axis of a classical magnetic moment for which a single measurement could take any value between $+\mu_s$ and $-\mu_s$ where μ_s is the total magnetic moment. Thus, if our Hamiltonian is a function of \hat{S}_z only, then the partition function corresponding to the classical measurement of said quantum system is given as a sum over the eigenstates of this Hamiltonian, rather than an integral over the quantum manifold of states,

$$\mathcal{Z} \equiv \text{Tr}(e^{-\beta \hat{H}}) = \sum_{m=-s}^s \langle s, m | e^{-\beta \hat{H}[\hat{S}_z]} | s, m \rangle. \quad (8)$$

One way to sample the partition function over the quantum space of states is to recast the system in terms of the so-called spin coherent states¹⁷. Indeed, not only do the spin coherent states form a continuous basis for the spin system, enabling a mapping onto the continuous description in terms of a unit vector living on a sphere, but it has also been shown that their behavior is close to the classical limit¹⁸. Thus, they enable us to efficiently sample the manifold of quantum states, in a way that can offer hints as to the properties of the classical limit. The spin coherent states have previously been used to study fundamental aspects such as emerging supersymmetry in spin systems¹⁹, semiclassical transition probabilities²⁰, and energy gap computations within mean-field quantum perturbation theory²¹.

To use the spin coherent states, we work as follows: for a given quantum spin number s , we set

$$|p\rangle \equiv |s, s-p\rangle, \quad (9)$$

where $p \in \{0, 1, \dots, 2s-1, 2s\}$ using the labeling introduced above and we define the spin coherent states $|z\rangle$, labeled by a complex number z , by the action of the lowering operator²², $\hat{S}_- = \hat{S}_x - i\hat{S}_y$, as

$$|z\rangle \equiv (1 + |z|^2)^{-s} e^{z\hat{S}_-/\hbar} |0\rangle \quad (10)$$

where the $1/\hbar$ factor is a bookkeeping device needed to keep the exponential dimensionless. The action of \hat{S}_+ , \hat{S}_- and \hat{S}_z on $|p\rangle$ produces

$$\begin{aligned} \hat{S}_- |p\rangle &= \hbar\sqrt{(2s-p)(p+1)} |p+1\rangle \\ \hat{S}_+ |p\rangle &= \hbar\sqrt{p(2s-p+1)} |p-1\rangle \\ \hat{S}_z |p\rangle &= \hbar(s-p) |p\rangle. \end{aligned} \quad (11)$$

The expression in (10) is equivalent to

$$|z\rangle \equiv (1 + |z|^2)^{-s} \sum_{p=0}^{2s} \binom{2s}{p}^{1/2} z^p |p\rangle, \quad (12)$$

which, as we shall see, is more convenient for computing the action of spin operators on the spin coherent states. In this basis, we can write the partition function (8) as an integral over the complex label z for the spin coherent states as

$$\mathcal{Z} = \int d\mu(z) \langle z | e^{-\beta\hat{H}} | z \rangle \quad (13)$$

where the measure must be properly normalized as $\int d\mu(z) |z\rangle \langle z| = 1$. In this case

$$d\mu(z) = \frac{2s+1}{\pi} \frac{dz}{(1+|z|^2)^2}. \quad (14)$$

To study the quantum system close to the classical limit, we must calculate the matrix elements of \hat{S}_z and its powers on the states $|z\rangle$. The first two powers are

$$\langle z | \hat{S}_z | z \rangle = \hbar s \frac{1 - |z|^2}{1 + |z|^2} \quad (15)$$

$$\langle z | \hat{S}_z^2 | z \rangle = \left(\hbar s \frac{1 - |z|^2}{1 + |z|^2} \right)^2 + 2\hbar^2 s \frac{|z|^2}{(1 + |z|^2)^2}. \quad (16)$$

In general, it can be shown that the higher-order terms are all of the form

$$\langle z | \hat{S}_z^k | z \rangle = \left(\hbar s \frac{1 - |z|^2}{1 + |z|^2} \right)^k + \text{noncommutative terms}. \quad (17)$$

The first term is the leading term in the classical limit. Noncommutative terms occur because \hat{S}_z and \hat{S}_\pm do not commute. The second term in (16) is an example, but there is no general closed expression for the correction of higher-order powers. These noncommutative terms describe the contribution

of the curvature of the sphere of quantum states, essentially the difference in the trajectory between states on a flat surface compared to a curved surface. However, the noncommutative terms are always of the same order in \hbar as the leading term. Thus neglecting the noncommutative terms does not simply correspond to the semi-classical \hbar expansion and needs to be justified differently. We remark that by setting $\hbar s \equiv s$, equation (16) can be written as

$$\begin{aligned} \langle z | \hat{S}_z | z \rangle &= \hbar s \frac{1 - |z|^2}{1 + |z|^2} = s \frac{1 - |z|^2}{1 + |z|^2} \\ \langle z | \hat{S}_z^2 | z \rangle &= \left(\hbar s \frac{1 - |z|^2}{1 + |z|^2} \right)^2 + 2\hbar^2 s \frac{|z|^2}{(1 + |z|^2)^2} = \\ &= s^2 \left\{ \left(\frac{1 - |z|^2}{1 + |z|^2} \right)^2 + 2 \frac{|z|^2}{s(1 + |z|^2)^2} \right\}, \end{aligned} \quad (18)$$

which highlights the property that the noncommutative terms, which are sensitive to the curvature of the manifold of spin superpositions, are of higher order in an $1/s$ expansion; and that the operators, that have a sensible large-spin, i.e. semi-classical, limit are \hat{S}_z^k/s^k . Indeed, this limit entails taking $\hbar \rightarrow 0$, $s \rightarrow \infty$ while keeping the product, $s \equiv \hbar s$ fixed.

In our case, which terms are to be neglected will depend on both this first expansion, and the β series expansion of $e^{-\beta\hat{H}}$ in the partition function. The second expansion being in powers of β , it is a high temperature expansion. However, it is not a Taylor expansion around a given value; thus, higher orders of β will improve the temperature range and convergence towards the quantum solution, and technically going to an infinite order in β yields the exact quantum solution.

When ignoring the noncommutative terms, we can rewrite the first term on the right-hand side of (17) as an exponential series

$$\sum_{k=0}^{\infty} \frac{1}{k!} \langle z | \hat{S}_z^k | z \rangle \approx \exp \left(\hbar s \frac{1 - |z|^2}{1 + |z|^2} \right), \quad (19)$$

and this will be shown later to yield the classical limit.

We now define the Hamiltonian for a single spin (whose electromagnetic properties will be described by its g -factor) in an applied magnetic field that is constant along the z -direction,

$$\hat{H} = -\frac{g\mu_B}{\hbar} \hat{S}_z B_z \quad (20)$$

For the electron, $g \approx 2.002 = |g_e|$ is the absolute value of the electron g -factor, $\mu_B = 9.274 \times 10^{-23}$ J/T is the Bohr magneton, $\hbar = 1.05457182 \times 10^{-34}$ J/K is Planck's constant and B_z is the applied magnetic field in Tesla. Choosing a fixed field direction (which can always be taken to be along z) simplifies the calculation by reducing the noncommutativity as we work with the exponential of operators.

To compute the partition function, we again express the exponential as a series

$$\exp(-\beta\hat{H}) = \sum_{k=0}^{\infty} \frac{1}{k!} \left(\beta \frac{g\mu_B}{\hbar} \hat{S}_z B_z \right)^k, \quad (21)$$

and compute the matrix elements $\langle z | \exp(-\beta\hat{\mathcal{H}}) | z \rangle$, which, using equation (19), can be approximated by

$$\langle z | \exp(-\beta\hat{\mathcal{H}}) | z \rangle \approx \sum_{k=0}^{\infty} \frac{1}{k!} \left(\beta \frac{g\mu_B}{\hbar} \right)^k \left(\hbar s \frac{1 - |z|^2}{1 + |z|^2} \right)^k B_z^k. \quad (22)$$

Thus, the matrix elements take the simple form

$$\langle z | \exp(-\beta\hat{\mathcal{H}}) | z \rangle \approx \exp \left(\beta g\mu_B B_z s \frac{1 - |z|^2}{1 + |z|^2} \right). \quad (23)$$

The complex value z (and its conjugate \bar{z}) can then be mapped onto a unit 2-sphere by defining a unit *spin coherent state vector*²³, \mathbf{n} , with components

$$\begin{aligned} n_x &= \frac{z + \bar{z}}{1 + |z|^2} \\ n_y &= -i \frac{z - \bar{z}}{1 + |z|^2} \\ n_z &= \frac{1 - |z|^2}{1 + |z|^2}, \end{aligned} \quad (24)$$

and using this we can rewrite the matrix elements (23) as

$$\langle z | \exp(-\beta\hat{\mathcal{H}}) | z \rangle \approx \exp(\beta g\mu_B B_z s n_z). \quad (25)$$

This leads immediately to the definition of an equivalent classical Hamiltonian

$$\mathcal{H}_{\text{eff}} = -g\mu_B B_z s n_z = -\mu_s \mathbf{B} \cdot \mathbf{S}, \quad (26)$$

where we identify $\mathbf{S} = \mathbf{n}$ as the classical spin vector (magnetic moment) with length $\mu_s = sg\mu_B$. This recovers the classical precession of a magnetic moment in a magnetic field. Therefore, dropping the noncommutative terms, yields the expected classical limit of this quantum system. We emphasize that *all* the powers of \hat{S}_z^k are needed to recover the classical limit—only the noncommutative terms have been dropped. As we go to the large-spin limit, since the radius of the sphere is proportional to $1/s$, it becomes smaller and smaller, which justifies neglecting these terms.

The vector \mathbf{n} defined by the spin coherent states plays the role of the spin unit vector, which is commonly used in classical Heisenberg spin models. Thus, not only does the spin coherent states basis provide us with a continuous (integral) description of the quantum system, but it also yields a straightforward interpretation of the quantum system (described by its states and operators) in terms of the continuous classical system (described by the magnetization vector).

We shall now use the partition function in the spin coherent state basis to compute expectation values for the quantum spin Hamiltonian, close to the classical limit, by performing an expansion in increasing orders of β . We shall then compare these results to direct numerical calculations.

II. PARTITION FUNCTION AND EXPECTATION VALUES

The expectation value of an operator \hat{O} for the discrete quantum spin system is

$$\langle \hat{O} \rangle = \frac{\sum_{m=-s}^s \langle s, m | \hat{O} \exp(-\beta\hat{\mathcal{H}}) | s, m \rangle}{\sum_{m=-s}^s \langle s, m | \exp(-\beta\hat{\mathcal{H}}) | s, m \rangle}, \quad (27)$$

where the denominator is the partition function (8). In the spin coherent state basis, the expectation value is expressed in terms of integrals, rather than sums, *viz.*

$$\langle \hat{O} \rangle = \frac{\int d\mu(z) \langle z | \hat{O} \exp(-\beta\hat{\mathcal{H}}) | z \rangle}{\int d\mu(z) \langle z | \exp(-\beta\hat{\mathcal{H}}) | z \rangle}. \quad (28)$$

As mentioned above, the spin coherent states are not eigenstates of \hat{S}_z , making the exponentiation more subtle. The action of the exponential of \hat{S}_z on $|s, m\rangle$ simply yields the exponentiation of the eigenvalue

$$e^{\hat{S}_z/\hbar} |s, m\rangle = e^m |s, m\rangle; \quad (29)$$

but in the spin coherent state basis, we cannot exactly compute the action and must resort to approximations such as the $1/s$ expansion and the high- and low-temperature expansions.

We proceed by calculating the expectation value $\langle \hat{S}_z \rangle$ as a function of temperature with the Zeeman Hamiltonian (20). This is known to be qualitatively different for classical and quantum spin models due to spin quantisation²⁴. The expectation value $\langle \hat{S}_z \rangle$ can be identified with the magnetization induced by an external field (in the limit when the exchange interaction can be neglected).

The exact quantum expectation value, calculated from the discrete basis, where the action of $\hat{S}_z |s, m\rangle = \hbar m |s, m\rangle$, gives

$$\langle \hat{S}_z \rangle = \frac{\sum_{m=-s}^s \hbar m \exp(\beta g\mu_B m B_z)}{\sum_{m=-s}^s \exp(\beta g\mu_B m B_z)}. \quad (30)$$

The expectation value in the classical limit is calculated with the spin coherent states using equation (28) and the approximation in equation (23) which neglects the terms proportional to powers of $1/s$, yielding

$$\langle \hat{S}_z \rangle \approx \hbar s \frac{\int dz \frac{1 - |z|^2}{(1 + |z|^2)^3} \exp \left(\beta g\mu_B B_z s \frac{1 - |z|^2}{1 + |z|^2} \right)}{\int dz \frac{1}{(1 + |z|^2)^2} \exp \left(\beta g\mu_B B_z s \frac{1 - |z|^2}{1 + |z|^2} \right)}. \quad (31)$$

Using these expressions for the discrete quantum model (30) and the classical limit of the spin coherent state (31), we plot the expectation value $\langle \hat{S}_z \rangle$ as a function of temperature in Figure 1. Neglecting the terms due to the non-comutativity of

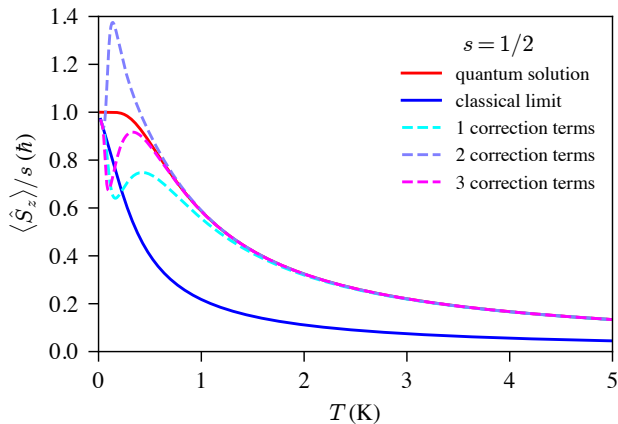


FIG. 1. Expectation value $\langle \hat{S}_z \rangle$ for spin $s = 1/2$ as a function of temperature. Red solid line - the exact quantum solution in the discrete spin basis $|s, m\rangle$ from Eq. (30). Blue solid line - the classical limit of the spin coherent state basis from Eq. (31). Dashed lines are successive corrections to the partition function to include non-commutative terms such as appear in Eq. (16). The applied field is $B_z = 1$ T for all figures.

\hat{S}_z and \hat{S}_\pm , i.e. working to leading order in the $1/s$ expansion, means the representation by the spin coherent states produces the classical limit (blue solid line), as expected, with an immediate decay of the spin alignment with the external field as soon as the temperature is non-zero. Equation (31) is, in fact, identical to the expectation value $\langle S_z \rangle$ of a classical spin, as is expected from Ehrenfest's theorem—a useful sanity check (see Appendix A). In the quantum case (red solid line) the expectation value remains almost flat—at low temperatures—and displays a slower characteristic decay around the zero temperature value, along with an initial inflection point that is expected on general grounds⁷.

These characteristic differences between quantum and classical models of single spins are well known and well studied. Of practical interest is that we can obtain an *intermediate* approximation for the quantum expectation value by retaining terms related to the commutation of operators. This pulls quantum features into the classical model in a rigorous manner. To do this, the exponential functions in the spin coherent state expectation value (28) must be expanded as a series in β ,

$$\exp(\beta \hbar \hat{S}_z) \approx 1 + \beta \hbar \hat{S}_z + \frac{1}{2} (\beta \hbar \hat{S}_z)^2 + \dots \quad (32)$$

Higher-order terms beyond \hat{S}_z contain the effects of the non-commutativity of operators, as seen in (16), and we now include these terms as we evaluate the expectation value. We calculate $\langle \hat{S}_z \rangle$ in the spin coherent state basis for increasing orders in the β expansion, which includes the terms due to noncommutativity of \hat{S}_z to higher orders. The results are shown with dashed lines in Figure 1. '1 correction term' includes \hat{S}_z^2 , '2 correction terms' \hat{S}_z^3 and so on. We see that including even the first noncommuting term in this expansion yields a solution that is already significantly different from the classical

result and close to the quantum solution at temperatures of the order of 1 K and above. The agreement improves as the temperature increases, as expected for an expansion in powers of β . Evaluating to higher orders in β causes the expectation value to converge more quickly to the quantum solution (Figure 1), thus producing a continuous description of the discrete quantum system, which is one of our main objectives.

For *very low* temperatures, close to 0 K, the approximation as a power series in β breaks down and diverges because β is the inverse of the temperature. We emphasize, however, that already at first order in β , this semi-classical model accurately captures the salient features of the thermal spin statistics of the quantum system at temperatures of the order of 1 K. Next, we build a numerical sampling technique for this path integral based on classical spin dynamics.

III. EFFECTIVE HAMILTONIAN AND ATOMISTIC SPIN DYNAMICS

A. Low-temperature expansion of the matrix elements

Building a classical Hamiltonian dynamics model to emulate a quantum system, expressed in the spin coherent states basis, requires finding an effective classical Hamiltonian \mathcal{H}_{eff} which approximates $\langle z | \exp(-\beta \hat{\mathcal{H}}) | z \rangle$ as $\exp(-\beta \mathcal{H}_{\text{eff}})$. By finding such an approximate expression, we recast the quantum system with partition function (8) into an effective classical system with partition function

$$\begin{aligned} \mathcal{Z} &= \int d\mu(z) \langle z | \exp(-\beta \hat{\mathcal{H}}) | z \rangle \\ &\approx \int d\tilde{\mu}(z) \exp(-\beta \mathcal{H}_{\text{eff}}), \end{aligned} \quad (33)$$

where \mathcal{H}_{eff} yields the same expectation values as for the quantum case and $\tilde{\mu}(z)$ describes a potentially enlarged, higher-dimensional, phase space, as is the case in path integral molecular dynamics approaches²⁵.

We consider the partition function with the first commutation correction (16), and seek an expression such that

$$\begin{aligned} \exp(-\beta \mathcal{H}_{\text{eff}}) &\approx \exp\left(\beta g \mu_B B_z s \frac{1 - |z|^2}{1 + |z|^2}\right) \\ &\quad + (\beta g \mu_B B_z)^2 \frac{|z|^2}{(1 + |z|^2)^2}, \end{aligned} \quad (34)$$

where the first term on the right-hand side is the classical limit and the second term is the first noncommutation term which appears on the right-hand side of (16). We ignore all higher-order non commutation terms in $\langle z | \hat{S}_z^k | z \rangle$, beyond $k = 2$. This is the same level of approximation used in '1 correction term' in Fig. 1. As a first and very coarse approximation (for more details, see appendix B) we take

$$\mathcal{H}_{\text{eff}}^{\text{low-T}} = -g \mu_B B_z s \frac{1 - |z|^2}{1 + |z|^2} + g \mu_B B_z \frac{\sqrt{2s}|z|}{1 + |z|^2}, \quad (35)$$

which, written in terms of the spin coherent state vector \mathbf{n} , is

$$\mathcal{H}_{\text{eff}}^{\text{low-T}} = -g\mu_B B_z s n_z + \frac{1}{2}g\mu_B B_z \sqrt{2s} \sqrt{1-n_z^2}. \quad (36)$$

The first term is again the purely classical Zeeman Hamiltonian (26). The second term arises due to the quantization of spin and energetically favors the spin to align with the quantization axis (z). It has a form similar to magnetocrystalline anisotropy, but its origin is the quantum behavior of the spin rather than any physical interaction. We will refer to this term as $\mathcal{H}_{\text{Qeff}}$.

To calculate the classical expectation values of this effective Hamiltonian, we use the techniques of atomistic spin dynamics (ASD)²⁶⁻³⁰. This is usually used to model the dynamics of localized spin magnetic moments $\boldsymbol{\mu} = \mu_s \mathbf{S}$ where \mathbf{S} is a unit vector and $\mu_s = gs\mu_B$ is the size of the spin magnetic moment. The moments interact with a local effective magnetic field \mathbf{B}_{eff} obtained from a Hamiltonian \mathcal{H}_{eff} that encodes the different magnetic interactions of the system. Here we will retain our use of the vector \mathbf{n} rather than \mathbf{S} to emphasize that we are solving the dynamics of the spin coherent state vector rather than making an *a priori* assumption of classical spin magnetic moments.

Calculations of the thermodynamic quantities of classical spins can be performed with ASD or Monte Carlo calculations, but ASD is trivial to parallelize across large ensembles of spins, allowing efficient calculation as well as the ability to calculate real-time dynamics. The classical spin dynamics is described by the Landau-Lifshitz-Gilbert (LLG) equation of motion

$$\dot{\mathbf{n}} = -\frac{\gamma}{1+\alpha^2} (\mathbf{n} \times \mathbf{B}_{\text{eff}} + \alpha \mathbf{n} \times (\mathbf{n} \times \mathbf{B}_{\text{eff}})), \quad (37)$$

where γ is the gyromagnetic ratio in $\text{rad} \cdot \text{s}^{-1} \cdot \text{T}^{-1}$, α is a dimensionless damping parameter, and the effective field \mathbf{B}_{eff} in Tesla is calculated as

$$\mathbf{B}_{\text{eff}} = -\frac{1}{\mu_s} \nabla_{\mathbf{n}} \mathcal{H}. \quad (38)$$

thus, the field from our effective Hamiltonian (36) is

$$\mathbf{B}_{\text{eff}}^{\text{low-T}} = B_z \mathbf{e}_z + \frac{\sqrt{2}}{2\sqrt{s}} B_z \frac{n_z}{\sqrt{n_x^2 + n_y^2}} \mathbf{e}_z, \quad (39)$$

where \mathbf{e}_z is the unit vector along z . This expression is apparently singular for $n_z = 1$; this singularity simply indicates that the magnetic field doesn't have any effect on a moment that is aligned with it; we realize, indeed, that such an initial condition, which must be treated separately, is very improbable at any finite temperature.

Temperature is included in the formalism by adding a stochastic field $\mathbf{B}_{\text{eff}} \rightarrow \mathbf{B}_{\text{eff}} + \boldsymbol{\eta}$ that turns the Landau-Lifshitz-Gilbert equation of motion (37) into a Langevin equation. The stochastic field is defined through the fluctuation dissipation theorem, which in the classical case requires $\boldsymbol{\eta}$ to be a white noise with the properties

$$\begin{aligned} \langle \eta_i(t) \rangle &= 0 \\ \langle \eta_i(t) \eta_j(t') \rangle &= \frac{2\alpha \delta_{ij} \delta(t-t')}{\beta \mu_s \gamma}, \end{aligned} \quad (40)$$

where i, j are Cartesian components. Recently, stochastic fields using the quantum fluctuation dissipation theorem have been used, enforcing a Bose-Einstein statistical distribution for the noise². This assumes that the relevant thermally occupied objects in this case are magnons, which should obey Planck statistics. Here, our work differs in that the quantum nature of the spin will be included directly into the effective field without making any assumption of the statistical distribution.

We numerically integrate the LLG equation (37) using a symplectic integration scheme³¹ with a timestep of 0.05 ps. The expectation values from the numerical method are calculated as averages over time and multiple realizations of the stochastic dynamics

$$\langle S_z \rangle = \frac{1}{N_s} \frac{1}{N_t} \sum_{i=1}^{N_s} \sum_{t=1}^{N_t} n_{i,z}(t), \quad (41)$$

where N_s is the number of independent spin trajectories and N_t is the number of time samples. The average in time is taken after an equilibration period where the system relaxes from the initial state to a thermalized state. The simulations performed here equilibrate within a few nanoseconds; therefore, we started the averaging procedure after an equilibration period of 5 ns. The averaging time is 15 ns and $N_s = 20$.

From the effective Hamiltonian (35), we compute the expectation values for \hat{S}_z , from the approximate partition function

$$\langle \hat{S}_z \rangle \approx \frac{\int d\mu(z) \hbar s \frac{1-|z|^2}{1+|z|^2} \exp(-\beta \mathcal{H}_{\text{eff}})}{\int d\mu(z) \exp(-\beta \mathcal{H}_{\text{eff}})}, \quad (42)$$

and compare these to the results we obtain from atomistic simulations of the same system. The results for different values of the principal quantum number $s = 1/2, 2, 5$ are shown in Figure 2.

All three models, classical, quantum and the effective Hamiltonian (42) converge to the same values in the high-temperature limit. In figure 2a for $s = 1/2$ the effective model only has small corrections to the classical model and the overall behavior is not close to the quantum solution. Only the slope at zero temperature shows any of the quantum behavior with a small inflection point. This is a feature which several effective models have attempted to force artificially on the studied spin systems to reproduce the experimental behavior for magnetization curves³². However, our model does not impose any hypotheses on the system and has no fitting parameters. The additional computational cost of making the classical system more closely resemble its quantum avatar is minimal, requiring only the addition of a field that amounts to an effective anisotropy.

Although this coarse approximation scheme provides results that are closer to the quantum results, there is no way to systematically improve the approximation scheme. For each higher-order commutation correction we must again try to derive a \mathcal{H}_{eff} ad hoc that satisfies equation (33). Therefore, we continue by developing a more systematic method for which computing the expectation values to higher orders of accuracy is straightforward.

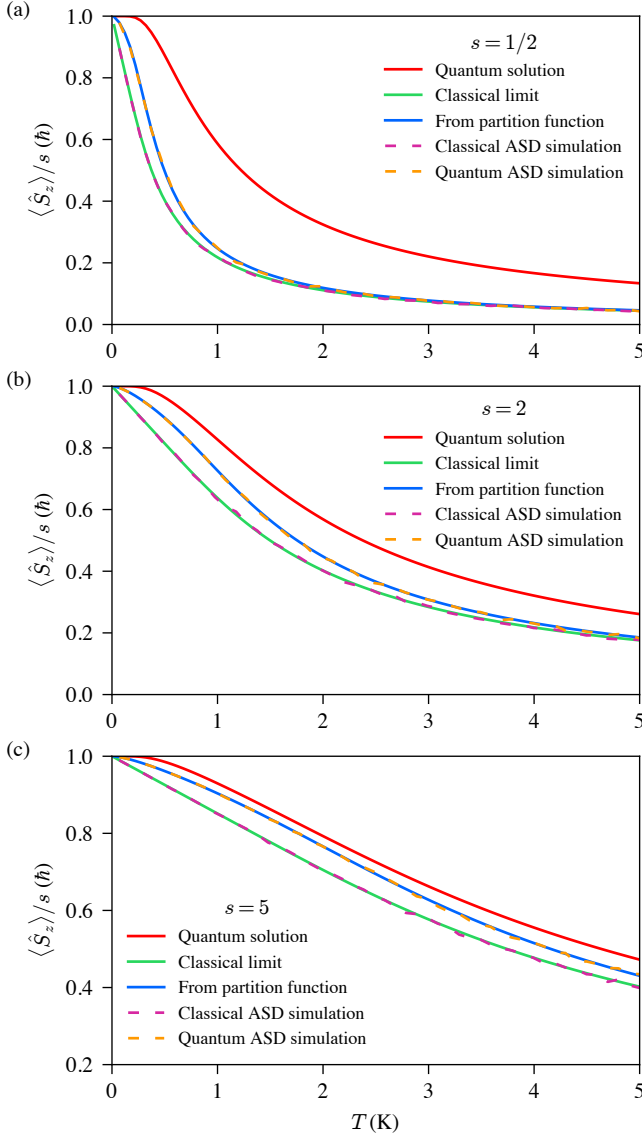


FIG. 2. Expectation value for \hat{S}_z as a function of temperature for the classical limit (green solid curve), quantum solution (red solid curve) and effective model (blue solid curve) from partition function. Equivalent results from enhanced atomistic spin dynamics simulation for classical limit (purple dashed curve) and effective model (orange dashed curve). (a) Top pane $s = 1/2$, (b) middle pane $s = 2$ and (c) bottom pane $s = 5$

B. High-temperature spin coherent states expansion

The effective model in the previous section produced by approximating the integrand of the partition function by an exponential is very coarse but yields some quantum corrections and at a very low computational cost. We now improve on this to try to recover a behavior more similar to the expansion of the partition function in Figure 1. We do this by including higher-order noncommutative terms in the expansion of $\exp(-\beta\hat{\mathcal{H}})$ (21) in a more systematic way.

We return to the partition function (13) and, similar to the path-integral molecular dynamics approaches, introduce the resolution of unity as

$$\sum_{p=0}^{2s} |p\rangle \langle p| = 1, \quad (43)$$

in the $|s, m\rangle$ basis, in which \hat{S}_z is diagonal, resulting in

$$\mathcal{Z} = \int \sum_{p=0}^{2s} d\mu(z) \langle z| e^{\frac{\beta g \mu_B}{\hbar} B_z \hat{S}_z} |p\rangle \langle p| z \rangle. \quad (44)$$

Using the definition of $|z\rangle$ and the action of \hat{S}_z on $|p\rangle$ we find

$$\mathcal{Z} = \int d\mu(z) \left[e^{-\beta g \mu_B s B_z} \left(\frac{e^{\beta g \mu_B B_z} + |z|^2}{1 + |z|^2} \right)^{2s} \right], \quad (45)$$

for which we need to rewrite the integrand

$$F[\beta, z] \equiv e^{-\beta g \mu_B s B_z} \left(\frac{e^{\beta g \mu_B B_z} + |z|^2}{1 + |z|^2} \right)^{2s}, \quad (46)$$

as a single exponential of the form $F[\beta, z] \equiv \exp(-\beta\mathcal{H}_{\text{eff}})$ to identify a Hamiltonian from which to construct an effective model. Through a series of identities (see appendix C), we can write

$$F[\beta, z] = \exp \left\{ 2s \left[\ln(2) + \ln \left(\frac{|z|}{1 + |z|^2} \right) + \ln \left(\cosh \left(e^{\frac{\beta g \mu_B B_z}{2}} - \ln(|z|) \right) \right) \right] \right\}. \quad (47)$$

We then approximate (47) with a Taylor expansion for $\beta \rightarrow 0$. Thus in the high-temperature limit (which we later find to be quite low)

$$\begin{aligned} \ln(F[\beta, z]) \approx & \frac{(1 - |z|^2) \beta g \mu_B s B_z}{1 + |z|^2} + \frac{|z|^2 \beta^2 (g \mu_B)^2 s B_z^2}{(1 + |z|^2)^2} \\ & - \frac{|z|^2 (1 - |z|^2) \beta^3 (g \mu_B)^3 s B_z^3}{3(1 + |z|^2)^3} + \mathcal{O}(\beta^4). \end{aligned} \quad (48)$$

Mapping to the spin coherent state vector components using $(1 - |z|^2)/(1 + |z|^2) = n_z$ and $|z|^2/(1 + |z|^2) = (1 - n_z^2)/4$, we can write a temperature-dependent effective Hamiltonian:

$$\begin{aligned} \mathcal{H}_{\text{eff}}^{\text{high-T}} \approx & -g \mu_B s B_z n_z - \frac{1}{4} \beta (g \mu_B)^2 s B_z^2 (1 - n_z^2) \\ & + \frac{1}{12} \beta^2 (g \mu_B)^3 s B_z^3 n_z (1 - n_z^2). \end{aligned} \quad (49)$$

From the temperature-dependent Hamiltonian (49) and the definition of the effective field (38), we derive

$$\mathbf{B}_{\text{eff}}^{\text{high-T}} = B_z - \frac{1}{2} \beta g \mu_B B_z^2 n_z - \frac{1}{12} \beta^2 (g \mu_B)^2 B_z^3 (1 - 3n_z^2). \quad (50)$$

We use this effective field in numerical atomistic simulations and compare with the expectation values computed directly from the partition function (42) and the relevant terms,

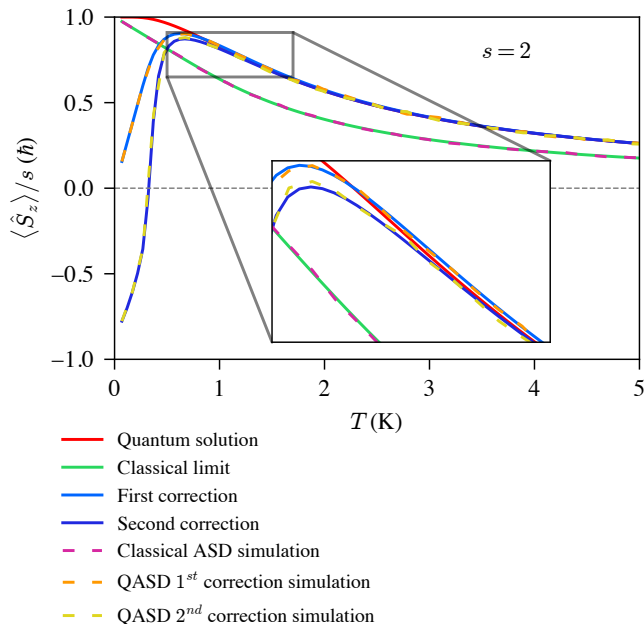


FIG. 3. Expectation value for \hat{S}_z for $s = 2$ as a function of temperature for classical limit (green solid curve) and quantum solution (red solid curve) and effective model with the first correction (light blue solid curve) and second correction (dark blue solid curve) from partition function. Equivalent results from enhanced atomistic spin dynamics simulation for classical limit (purple dashed curve) and second effective model with first correction (orange dashed curve) and second correction (yellow dashed curve)

according to the order of the approximation, of the effective Hamiltonian (49). The results are shown in Figure 3.

When we include only the first correction for the effective field, namely the first and second terms on the right-hand side of (49) then, contrary to the previous section (Figure 2), the low-temperature limit is far from both classical and quantum solutions. However, around 1 K, the results become very close to the quantum solution and converge to be almost identical as the temperature increases.

Including higher-order terms (for example, using all the terms in (50)) we see that although at low temperatures the model moves further away from the quantum solution, the rate of convergence towards it is much faster. For the first correction, once close to the quantum solution, it takes a while before both curves are indistinguishable, and this happens much quicker when including the second term (see the inset of Figure 3). As our approximation is computed to higher orders, the convergence becomes faster. We note that there is no reason why this high-temperature expansion should become valid at much lower temperatures as we go to higher orders.

The second drawback that we have to deal with is that these expectation curves have to be normalized in order for the atomistic simulations to overlap with the direct computation from the partition function. Indeed, when we compute the expectation value for $\langle \hat{S}_z \rangle$ we should be using an expression of

the form of Eq. (28) as

$$\langle \hat{S}_z \rangle \approx \frac{\int d\mu(z) \langle z | \hat{S}_z \exp\left(\frac{\beta g \mu_B}{\hbar} B_z \hat{S}_z\right) | z \rangle}{\int d\mu(z) e^{-\beta \mu_s B_z} \left(\frac{e^{\beta g \mu_B B_z + |z|^2}}{1 + |z|^2}\right)^{2s}}, \quad (51)$$

but instead (see appendix D), we define

$$\langle \hat{S}_z \rangle_{\text{app}} \equiv \frac{\int d\mu(z) \hbar s \frac{1 - |z|^2}{1 + |z|^2} e^{-\beta \mu_s B_z} \left(\frac{e^{\beta g \mu_B B_z + |z|^2}}{1 + |z|^2}\right)^{2s}}{\int d\mu(z) e^{-\beta \mu_s B_z} \left(\frac{e^{\beta g \mu_B B_z + |z|^2}}{1 + |z|^2}\right)^{2s}}. \quad (52)$$

We know that in the quantum case given by Eq. (30), $\langle \hat{S}_z \rangle_{\text{quantum}}$ goes to s as $\beta \rightarrow \infty$. We can show that in the same limit, for Eq. (D3), we have

$$\langle \hat{S}_z \rangle_{\text{app}} \xrightarrow{\beta \rightarrow \infty} \frac{s^2}{s + 1} \quad (53)$$

hence our expectation values need to be normalized by this factor to yield the correct results (see appendix D for more details).

In summary, using this approximation scheme, we can compute expectation values for the quantum system from an equivalent classical atomistic simulation where the quantum nature of the system is represented by a *temperature-dependent* effective field. In contrast to the previous section (III A), these then need to be properly rescaled. However, we can compute a closed expression for this rescaling factor, which once again depends only on the principal quantum spin number s . Once this step is fulfilled, the results are almost identical to the fully quantum expectation values for high enough temperatures, which are of the order of 1 K for the single spin in a magnetic field studied here. The low-temperature behavior of this scheme is not as well behaved as in Section III A, which is not surprising, as this is a high-temperature expansion (see Appendix E).

IV. CONCLUSION

In this Article, we have built an effective, classical, dynamical model for quantum spin systems from a path integral approach inspired by path integral molecular dynamics in the simplest case of a single spin of arbitrary size in a constant magnetic field described by a Zeeman Hamiltonian. While path integral models of spin have a long history and have been investigated in fundamental contexts such as supersymmetry or, more closely related to our work for molecular magnets, a systematic approach bridging the gap from small-size fully quantum simulations to large-scale dynamical simulations with quantum features has been lacking. Our work here is the first step towards this direction.

We have started by expressing the partition function for spin systems in the spin coherent state basis to obtain a continuous description in terms of an integral rather than a sum, to make the connection to classical spin dynamics. This allows the use of highly efficient atomistic spin dynamics simulations

for quantum spin systems and makes the connection between the quantum system defined by its states and the Hamiltonian operator and classical spin dynamics more explicit. We then proceeded to expand the relevant matrix elements of the partition function in powers of β to compute the expectation values of \hat{S}_z directly from the partition function and from atomistic spin dynamics. Here, we have seen that in this first approximation this could be done very simply and efficiently by adding an anisotropic effective field, which could be directly inferred from the quantum spin number of the system. For small spin values, we have seen that the improvement is quite small but increases with the spin. Of course, spin $s = 1/2$ represents the most extreme limit of spin quantization. As the magnitude of the spin increases to $s = 2$ and $s = 5$ (Fig. 2b,c) the corrections in the effective model take the system closer to the quantum solution. Many magnetic materials of practical relevance have s in the range $3/2$ to $7/2$ so having an improved quantum description for these larger spin values is already very useful.

We also investigated a different method of approximating the integrand of the partition function by an exponential by allowing the effective Hamiltonian of the system to be explicitly temperature-dependent, yielding a temperature-dependent effective field for describing in this way the quantum nature of the system. This method proved to be more accurate for higher temperatures, above 1 K, than the low-temperature expansion, but with the drawback that the expectation values computed using this method require renormalization. However, this renormalization factor has a closed general expression that depends only on the quantum spin number s of the system.

The next step we aim to investigate is the more general case of a general, time-dependent, magnetic field. This introduces more noncommutativity issues with operators \hat{S}_x , \hat{S}_y and \hat{S}_\pm . Beyond this more complex Hamiltonians including the exchange interaction and magnetocrystalline anisotropy in a quantum fashion will allow the large-scale calculation of the thermodynamics of magnetic materials including quantum effects with a relatively low computational cost. In the present case of a constant magnetic field and for a single spin, we have seen that, conversely to path integral methods for molecular dynamics, we did not need to introduce copies of the spin which interact with itself. We do not expect this to hold in more complex Hamiltonians.

DATA ACCESS

Python code and output data to reproduce all results and figures reported in this paper are openly available from the Zenodo repository: *Sources for: Numerical Simulations of a Spin Dynamics Model Based on a Path Integral Approach*. <https://doi.org/10.5281/zenodo.7688972>³³. The repository contains:

- Python code to generate analytic equations derived herein.
- Python code to perform enhanced atomistic spin dynamics calculations with the quantum effective fields.

- Python scripts to reproduce all figures.

The software and data are available under the terms of the MIT License.

AUTHOR CONTRIBUTIONS

Thomas Nussle: conceptualization, methodology, investigation, software, writing - original draft. Stam Nicolis: methodology, writing - review and editing. Joseph Barker: conceptualization, methodology, software, data curation, writing - review and editing, funding acquisition.

ACKNOWLEDGMENTS

This work was supported by the Engineering and Physical Sciences Research Council [grant number EP/V037935/1]. JB acknowledges funding from a Royal Society University Research Fellowship. The authors thank A. Sylla, F. Labéy and T. Raujouan for very insightful mathematical discussions, as well as J. Hodrien and A. Coleman from the University of Leeds Research Computing team for their help with optimizing the Python code on which this work is relying.

Appendix A: Correspondence of the spin coherent states with the classical limit

Here we show that the observable $\langle \hat{S}_z \rangle$ from the spin coherent states with the commutators neglected (i.e. in the classical limit (31)) is identical to $\langle S_z \rangle$ calculated from the classical Heisenberg model. For a classical Heisenberg spin with Hamiltonian

$$\mathcal{H} = -\mu_s \mathbf{B} \cdot \mathbf{S}, \quad (\text{A1})$$

where \mathbf{S} lives on the unit sphere, the partition function is

$$\mathcal{Z} = \int d\mathbf{S} \delta(\mathbf{S}^2 - 1) e^{-\beta \mathcal{H}} = \int d\mathbf{S} \delta(\mathbf{S}^2 - 1) e^{\beta \mu_s \mathbf{B} \cdot \mathbf{S}}, \quad (\text{A2})$$

for which the expectation value of the z -component of \mathbf{S} is given by

$$\langle S_z \rangle = \frac{\int d\mathbf{S} \delta(\mathbf{S}^2 - 1) S_z e^{\beta \mu_s \mathbf{B} \cdot \mathbf{S}}}{\int d\mathbf{S} \delta(\mathbf{S}^2 - 1) e^{\beta \mu_s \mathbf{B} \cdot \mathbf{S}}}. \quad (\text{A3})$$

If the external field is constant along the z -direction then we have

$$\langle S_z \rangle = \frac{\int dS_x dS_y dS_z S_z e^{\beta \mu_s B_z S_z}}{\int dS_x dS_y dS_z e^{\beta \mu_s B_z S_z}} \quad (\text{A4})$$

as the integrals over S_x and S_y in the numerator and denominator cancel each other out. Comparing this to $\langle \hat{S}_z \rangle$ for the

spin coherent state (31) and using $n_z = (1 - |z|^2)/(1 + |z|^2)$ and $\mu_s S_z = g s \mu_B n_z$ we see that (A4) and (31) are identical up to a factor of \hbar , as the classical spin vector has no units, whereas the quantum expectation value of $\langle \hat{S}_z \rangle$ is in units of \hbar .

Appendix B: Coarse approximation method

We expand the operator exponential series (21) up to second order in β

$$\begin{aligned} \exp(-\beta \hat{\mathcal{H}}) &\approx 1 + \beta g \mu_B B_z s \frac{1 - |z|^2}{1 + |z|^2} \\ &+ \beta^2 (g \mu_B B_z)^2 \frac{s |z|^2}{(1 + |z|^2)^2} \\ &+ \frac{1}{2} \left(\beta g \mu_B B_z s \frac{1 - |z|^2}{1 + |z|^2} \right)^2, \end{aligned} \quad (\text{B1})$$

we can show that by taking

$$\mathcal{H}_{\text{eff}} = -g \mu_B B_z s \frac{1 - |z|^2}{1 + |z|^2} + g \mu_B B_z \frac{\sqrt{2s} |z|}{1 + |z|^2}, \quad (\text{B2})$$

and expanding the effective classical exponential up to the same order in β , we get

$$\begin{aligned} \exp(-\beta \mathcal{H}_{\text{eff}}) &\approx 1 + \beta g \mu_B B_z s \frac{1 - |z|^2}{1 + |z|^2} + \beta^2 (g \mu_B B_z)^2 \frac{s |z|^2}{(1 + |z|^2)^2} \\ &+ \frac{1}{2} \left(\beta g \mu_B B_z s \frac{1 - |z|^2}{1 + |z|^2} \right)^2 \\ &- \beta g \mu_B B_z \frac{\sqrt{2s} |z|}{1 + |z|^2} - (\beta g \mu_B B_z)^2 \frac{s \sqrt{2s} |z| (1 - |z|^2)}{(1 + |z|^2)^2}. \end{aligned} \quad (\text{B3})$$

This is where our approximation becomes more qualitative than quantitative. Indeed, the fifth and sixth terms on the right-hand side of (B3) are not present in (B1) even though they are not of higher order in β , however, we have taken advantage of the freedom of choice for the sign of the extra term in the effective Hamiltonian (second term on the right-hand side of (B2)) as the correction (third term on the right-hand side of (B1)) comes from the square term in the exponential series. Taking the correction (second term on the right-hand side of (B2)) to be negative implies that

$$\exp \left(-\beta g \mu_B B_z \frac{\sqrt{2s} |z|}{1 + |z|^2} \right) \in [0, 1], \quad (\text{B4})$$

or in terms of the spin coherent state vector

$$\exp \left(-\beta \frac{1}{2} g \mu_B B_z \sqrt{2s} \sqrt{1 - n_z^2} \right) \in [0, 1], \quad (\text{B5})$$

which means that our expectation value remains close to the classical expectation value, especially for lower temperatures where the spin preferentially aligns with the z -axis. Although this constitutes quite a coarse approximation, it is definitely a relevant primer to understand the subtleties of the path integral spin dynamics method.

Appendix C: High temperature model exponential form

Starting from (46), we rewrite

$$\begin{aligned} \left(\frac{e^{\beta g \mu_B B_z} + |z|^2}{1 + |z|^2} \right)^{2s} &= \left(\frac{e^{\beta g \mu_B B_z} + e^{2 \ln(|z|)}}{e^{\ln(1 + |z|^2)}} \right)^{2s} \\ &= \left(\frac{e^{\frac{\beta g \mu_B B_z}{2} + \ln(|z|)} \left(e^{\frac{\beta g \mu_B B_z}{2} - \ln(|z|)} + e^{-\frac{\beta g \mu_B B_z}{2} + \ln(|z|)} \right)}{e^{\ln(1 + |z|^2)}} \right)^{2s} \\ &= \left(\frac{e^{\frac{\beta g \mu_B B_z}{2} + \ln(|z|)} 2 \cosh \left(\frac{\beta g \mu_B B_z}{2} - \ln(|z|) \right)}{e^{\ln(1 + |z|^2)}} \right)^{2s} \\ &= \left(e^{\frac{\beta g \mu_B B_z}{2} + \ln \left(\frac{|z|}{1 + |z|^2} \right) + \ln \left(2 \cosh \left(\frac{\beta g \mu_B B_z}{2} - \ln(|z|) \right) \right)} \right)^{2s}, \end{aligned} \quad (\text{C1})$$

hence (46) can be rewritten as

$$F[\beta, z] = e^{2s \left(\ln(2) + \ln \left(\frac{|z|}{1 + |z|^2} \right) + \ln \left(\cosh \left(\frac{\beta g \mu_B B_z}{2} - \ln(|z|) \right) \right) \right)}. \quad (\text{C2})$$

Appendix D: High-temperature model normalization

We approximate

$$\begin{aligned} \langle z | \hat{S}_z \exp \left(\frac{\beta \mu_s}{\hbar} B_z \hat{S}_z \right) | z \rangle &\approx \langle z | \hat{S}_z | z \rangle \langle z | \exp \left(\frac{\beta \mu_s}{\hbar} B_z \hat{S}_z \right) | z \rangle \\ &= \hbar s \frac{1 - |z|^2}{1 + |z|^2} e^{-\beta \mu_s B_z s} \left(\frac{e^{\beta \mu_s B_z} + |z|^2}{1 + |z|^2} \right)^{2s}, \end{aligned} \quad (\text{D1})$$

as our approximation scheme for the partition function aims to move from a quantum description in terms of states and operators to a classical description

$$\langle z | \exp \left(\frac{\beta \mu_s}{\hbar} B_z \hat{S}_z \right) | z \rangle \approx \exp(-\beta \mathcal{H}). \quad (\text{D2})$$

Within this approximation, we can rewrite

$$\begin{aligned} &\frac{\int d\mu(z) \langle z | \hat{S}_z \exp \left(\frac{\beta \mu_s}{\hbar} B_z \hat{S}_z \right) | z \rangle}{\int d\mu(z) e^{-\beta \mu_s B_z s} \left(\frac{e^{\beta \mu_s B_z} + |z|^2}{1 + |z|^2} \right)^{2s}} \\ &\equiv \frac{\int d\mu(z) \hbar s \frac{1 - |z|^2}{1 + |z|^2} e^{-\beta \mu_s B_z s} \left(\frac{e^{\beta \mu_s B_z} + |z|^2}{1 + |z|^2} \right)^{2s}}{\int d\mu(z) e^{-\beta \mu_s B_z s} \left(\frac{e^{\beta \mu_s B_z} + |z|^2}{1 + |z|^2} \right)^{2s}}, \end{aligned} \quad (\text{D3})$$

which is the expression we use for our averages, as it corresponds to the same approximation as the atomistic model, as proven by the exact overlap of both the averages computed from the partition function (52) and the atomistic average over time and the number of realizations (41).

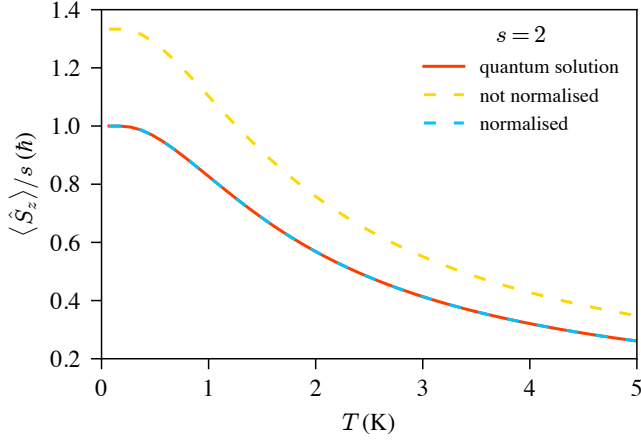


FIG. 4. Expectation value for \hat{S}_z for $s = 2$ as a function of temperature from (52) (orange dashed curve) and normalised according to (53) (cyan dashed curve) compared to the quantum limit (red solid curve)

What is of peculiar interest is that the ratio

$$\frac{\langle \hat{S}_z \rangle_{\text{app}}}{\langle \hat{S}_z \rangle_{\text{quantum}}} \xrightarrow{\beta \rightarrow \infty} \frac{s}{s+1} \quad (\text{D4})$$

which reminds us of the fact that the eigenvalues of \hat{S}^2 are $s(s+1)$ as in

$$\hat{S}^2 |s, m\rangle = s(s+1) |s, m\rangle \quad (\text{D5})$$

rather than simply s^2 . Indeed, in the classical limit $s \rightarrow \infty$ we recover

$$s(s+1) \xrightarrow{s \rightarrow \infty} s^2. \quad (\text{D6})$$

We would like to emphasize that this required normalization factor is identical for both the results of the atomistic simulations (41) and the results from the approximate partition function (52).

The expectation values for $\langle \hat{S}_z \rangle_{\text{app}}$ with and without normalization are given in Figure 4, along with the appropriate quantum solution.

This is very important for more general applications of this model as this means that the normalization of the curves does not require an additional fitting parameter of any kind but is rather analytically computable and has a general, closed expression.

Appendix E: Higher order correction for the high-temperature model

As mentioned in section III B our method can technically carry out this approximation scheme to any order in the non-commutative terms, numerically, without requiring to compute these corrections using pen and paper. But as this relies on a Taylor expansion around the high-temperature limit

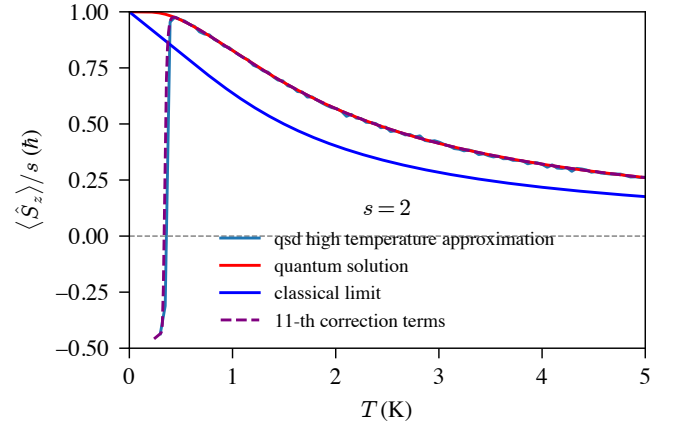


FIG. 5. Expectation value for \hat{S}_z for $s = 1/2$ as a function of temperature for classical limit (blue solid curve) and quantum solution (red solid curve) and effective model with the 10th correction (light blue solid curve) from partition function. Equivalent results from enhanced atomistic spin dynamics simulation effective model with 11th correction (purple dashed curve).

$\beta \rightarrow 0$ there is a limit as to how low in temperature we can provide accurate results. Indeed there is no reason for this high-temperature expansion to converge to the quantum solution for temperatures around 0 K. This is shown in Figure 5.

* t.s.nussle@leeds.ac.uk

† stam.nicolis@lmpt.univ-tours.fr

‡ j.barker@leeds.ac.uk

¹ David Ceperley and Berni Alder, “Quantum Monte Carlo,” *Science* **231**, 555–560 (1986).

² Joseph Barker and Gerrit E. W. Bauer, “Semiquantum thermodynamics of complex ferrimagnets,” *Phys. Rev. B* **100**, 140401 (2019).

³ Joseph Barker, Dimitar Pashov, and Jerome Jackson, “Electronic structure and finite temperature magnetism of yttrium iron garnet,” *Electron. Struct.* **2**, 044002 (2020).

net,” *Electron. Struct.* **2**, 044002 (2020).

⁴ C. H. Woo, Haohua Wen, A. A. Semenov, S. L. Dudarev, and Pui-Wai Ma, “Quantum heat bath for spin-lattice dynamics,” *Phys. Rev. B* **91**, 104306 (2015).

⁵ Lars Bergqvist and Anders Bergman, “Realistic finite temperature simulations of magnetic systems using quantum statistics,” *Phys. Rev. Mater.* **2**, 013802 (2018).

⁶ R. F. L. Evans, U. Atxitia, and R. W. Chantrell, “Quantitative simulation of temperature-dependent magnetization dynamics and equilibrium properties of elemental ferromagnets,” *Phys.*

- Rev. B **91**, 144425 (2015).
- ⁷ J Anders, C R J Sait, and S A R Horsley, “Quantum Brownian motion for magnets,” *New J. Phys.* **24**, 033020 (2022).
 - ⁸ Flynn Walsh, Mark Asta, and Lin-Wang Wang, “Realistic magnetic thermodynamics by local quantization of a semiclassical Heisenberg model,” *npj Comput. Mater.* **8**, 186 (2022).
 - ⁹ O. G. Shpyrko, E. D. Isaacs, J. M. Logan, Yejun Feng, G. Aeppli, R. Jaramillo, H. C. Kim, T. F. Rosenbaum, P. Zschack, M. Sprung, S. Narayanan, and A. R. Sandy, “Direct measurement of antiferromagnetic domain fluctuations,” *Nature* **447**, 68–71 (2007).
 - ¹⁰ M. Parrinello and A. Rahman, “Study of an F center in molten KCl,” *J. Chem. Phys.* **80**, 860–867 (1984).
 - ¹¹ Scott Habershon, David E. Manolopoulos, Thomas E. Markland, and Thomas F. Miller, “Ring-Polymer Molecular Dynamics: Quantum Effects in Chemical Dynamics from Classical Trajectories in an Extended Phase Space,” *Annu. Rev. Phys. Chem.* **64**, 387–413 (2013).
 - ¹² Johan E. Runeson and Jeremy O. Richardson, “Generalized spin mapping for quantum-classical dynamics,” *J. Chem. Phys.* **152**, 084110 (2020).
 - ¹³ Eugenio Coronado, “Molecular magnetism: from chemical design to spin control in molecules, materials and devices,” *Nat. Rev. Mater.* **5**, 87–104 (2019).
 - ¹⁴ Duncan Bossion, Wenxiang Ying, Sutirtha N. Chowdhury, and Pengfei Huo, “Non-adiabatic mapping dynamics in the phase space of the $SU(N)$ Lie group,” *J. Chem. Phys.* **157**, 084105 (2022).
 - ¹⁵ Hao Zhang and Cristian D. Batista, “Classical spin dynamics based on $SU(N)$ coherent states,” *Phys. Rev. B* **104**, 104409 (2021).
 - ¹⁶ Walther Gerlach and Otto Stern, “Der experimentelle Nachweis der Richtungsquantelung im Magnetfeld,” *Zeitschrift für Physik* **9**, 349–352 (1922).
 - ¹⁷ J M Radcliffe, “Some properties of coherent spin states,” *J. Phys. A: Gen. Phys.* **4**, 313–323 (1971).
 - ¹⁸ Yen Lee Loh and Monica Kim, “Visualizing spin states using the spin coherent state representation,” *Am. J. Phys.* **83**, 30–35 (2015).
 - ¹⁹ Michael Stone, “Supersymmetry and the quantum mechanics of spin,” *Nucl. Phys. B* **314**, 557–586 (1989).
 - ²⁰ Michael Stone, Kee-Su Park, and Anupam Garg, “The semiclassical propagator for spin coherent states,” *J. Math. Phys.* **41**, 8025–8049 (2000).
 - ²¹ Yang Wei Koh, “Effects of dynamical paths on the energy gap and the corrections to the free energy in path integrals of mean-field quantum spin systems,” *Phys. Rev. B* **97**, 094417 (2018).
 - ²² Of course one can also define these in terms of the raising operator or any linear combination of these³⁴.
 - ²³ Naoum Karchev, “Path integral representation for spin systems,” arXiv:1211.4509 [cond-mat] (2012), arXiv:1211.4509 [cond-mat].
 - ²⁴ Walter Greiner, Ludwig Neise, and Horst Stöcker, *Thermodynamics and Statistical Mechanics* (Springer New York, 2000).
 - ²⁵ Pierre Deymier, Keith Runge, and Krishna Muralidharan, eds., *Multiscale Paradigms in Integrated Computational Materials Science and Engineering*, Springer Series in Materials Science, Vol. 226 (Springer International Publishing, Cham, 2016).
 - ²⁶ S. V. Halilov, H. Eschrig, A. Y. Perlov, and P. M. Oppeneer, “Adiabatic spin dynamics from spin-density-functional theory: Application to Fe, Co, and Ni,” *Phys. Rev. B* **58**, 293–302 (1998).
 - ²⁷ O. Chubykalo, R. Smirnov-Rueda, J.M. Gonzalez, M.A. Wongsam, R.W. Chantrell, and U. Nowak, “Brownian dynamics approach to interacting magnetic moments,” *J. Magn. Magn. Mater.* **266**, 28–35 (2003).
 - ²⁸ O. N Mryasov, U Nowak, K. Y Guslienko, and R. W Chantrell, “Temperature-dependent magnetic properties of FePt: Effective spin Hamiltonian model,” *Eur. Lett. (EPL)* **69**, 805–811 (2005).
 - ²⁹ B Skubic, J Hellsvik, L Nordström, and O Eriksson, “A method for atomistic spin dynamics simulations: implementation and examples,” *J. Phys.: Condens. Matter* **20**, 315203 (2008).
 - ³⁰ R F L Evans, W J Fan, P Chureemart, T A Ostler, M O A Ellis, and R W Chantrell, “Atomistic spin model simulations of magnetic nanomaterials,” *J. Phys.: Condens. Matter* **26**, 103202 (2014).
 - ³¹ Pascal Thibaudeau and David Beaujouan, “Thermostatting the atomic spin dynamics from controlled demons,” *Phys. A: Stat. Mech. its Appl.* **391**, 1963–1971 (2012).
 - ³² M. D. Kuz’min, “Shape of Temperature Dependence of Spontaneous Magnetization of Ferromagnets: Quantitative Analysis,” *Phys. Rev. Lett.* **94**, 107204 (2005).
 - ³³ Thomas Nussle, Stam Nicolis, and Joseph Barker, “Sources for: Numerical Simulations of a Spin Dynamics Model Based on a Path Integral Approach (v1.0.4) [Data set],” (2023), Zenodo.
 - ³⁴ Kae Nemoto, “Generalized coherent states for $SU(n)$ systems,” *J. Phys. A: Math. Gen.* **33**, 3493–3506 (2000).